Dalton Transactions

Evaluation of Attractive Interactions in the Second Coordination Sphere of Iron Complexes Containing Pendant Amines

Journal:	*Dalton Transactions*
Manuscript ID	DT-ART-02-2019-000708.R1
Article Type:	Paper
Date Submitted by the Author:	11-Mar-2019
Complete List of Authors:	Liao, Qian; Dalian University of Technology Liu, Tianbiao; Utah State University, Chemistry and Biochemistry Johnson, Samantha; Pacific Northwest National Laboratory, Chemical and Materials Sciences Klug, Christina; Pacific Northwest National Laboratory, Physical Sciences Division Wiedner, Eric ; Pacific Northwest National Laboratory, Physical Sciences Division Bullock, R.; Pacific Northwest National Laboratory, Chemical and Materials Sciences DuBois, Daniel; Pacific Northwest National Laboratory, Physical Sciences Division

Evaluation of Attractive Interactions in the Second Coordination Sphere of Iron Complexes Containing Pendant Amines

Qian Liao,[a, b] Tianbiao Liu,[a, c] Samantha I. Johnson,[a] Christina M. Klug,[a] Eric S. Wiedner,*[,a] R. Morris Bullock,[a] and Daniel L. DuBois [a, d]

[a] Center for Molecular Electrocatalysis, Pacific Northwest National Laboratory, P.O. Box 999, K2-57, Richland, WA 99352 United States. E-mail: eric.wiedner@pnnl.gov

[b] Current Affiliation: Zhang Dayu School of Chemistry, Dalian University of Technology, Dalian, China

[c] Current Affiliation: Department of Chemistry and Biochemistry, Utah State University, Logan, Utah, United States

[d] Retired

Abstract

The interactions between pendant amines in the second coordination sphere and ligands in the first coordination sphere are important for understanding the structures and reactivity of complexes containing $P^{R}_2N^{R'}_2$ ligands, which have been shown to be highly active H_2 oxidation/production catalysts. A series of $[Fe(P^{Ph}_2N^{Bn}_2)_2(X)(Y)]^{n+}$ complexes have been prepared and structurally characterized. These complexes have two different ligands with which the pendant amines of the diphosphine ligand can interact. The solid state structure of *cis*-$Fe(P^{Ph}_2N^{Bn}_2)_2Cl_2$ reveals that the six-membered rings adjacent to the P atoms are in a boat confirmation, resulting in close N•••P distances that suggests the P atoms have a greater affinity for the lone pair of electrons on the N atom than chloride ligands. Similarly, boat conformations are observed for both rings adjacent to the hydride ligands of *trans*-$[HFe(P^{Ph}_2N^{Bn}_2)_2(CH_3CN)]^+$ and *trans*-$HFe(P^{Ph}_2N^{Bn}_2)_2Cl$, resulting in short N•••H distances. Spectroscopic and computational studies of *trans*-$[HFe(P^{Ph}_2N^{Bn}_2)_2(CO)]^+$, *trans*-$[HFe(P^{Ph}_2N^{Bn}_2)(P^{Ph}_2N^{Bn}_2H)(CO)]^{2+}$, and *trans*-$[HFe(P^{Ph}_2N^{Bn}_2)_2(H_2)]^+$ indicate the complexes are more stable when the pendant amines in boat conformations are adjacent to the hydride ligand. These data suggest an attractor ordering of H^- > CO > H_2 > PR_3 > Cl^- ~ CH_3CN.

Introduction

Interactions between functional groups of the protein backbone of redox enzymes and the active site of a protein play an important role in determining their catalytic activity. Recent studies from our laboratory and others have shown that these interactions can have significant influences on synthetic molecular electrocatalysts for reactions such as H_2 production/oxidation,[1-8] O_2 reduction/H_2O oxidation,[9-12] CO_2 reduction,[13-18] formate oxidation,[19, 20] alcohol oxidation,[21-23] and nitrate/nitrite reduction.[24, 25] However, our understanding of interactions between ligands or substrates bound directly to the metal (*i.e.*, the first coordination sphere) and functional groups in the second coordination sphere is still limited. These interactions between s-block and p-block elements depend significantly on the coordination geometry and oxidation state of the transition metal, and other ligands in the first coordination sphere, factors that change during a catalytic cycle. As a result, the interactions of functional groups in the second coordination sphere with ligands in the first coordination sphere are dynamic during most catalytic processes, making structural studies difficult. More precise structural information regarding such interactions may be available from the study of non-catalytic systems that permit detailed structural and spectroscopic studies.

Previous studies from our laboratory have focused on the use of $P^R_2N^{R'}_2$ ligands, which are eight-membered cyclic diphosphine ligands that possess pendant amines in the second coordination sphere. Coordination of a $P^R_2N^{R'}_2$ ligand to a metal creates two six-membered rings, each of which can adopt a chair or boat conformation (Figure 1a). The vast majority of $M(P^R_2N^{R'}_2)$ complexes that have been crystallographically characterized display a chair-boat conformation in the solid state, while the boat-boat and chair-chair conformations are much less common.[26] Theoretical studies of four-coordinate $[Ni(P^R_2N^{R'}_2)_2]^{2+}$ complexes indicate that the chair-boat and boat-boat conformations differ in energy by 3 kcal/mol or less, while the chair-chair conformations are 6-12 kcal/mol higher in energy due to electronic repulsion of the lone pairs of the two N atoms.[27]

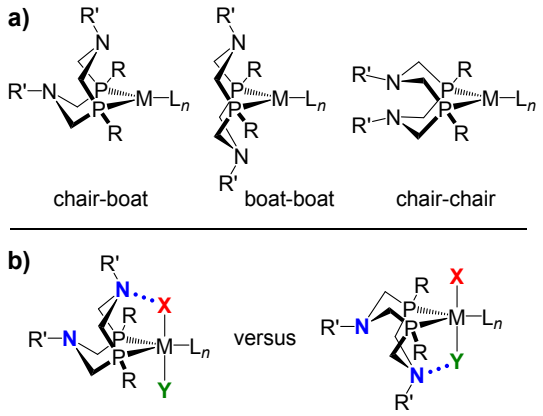

Figure 1. a) The common conformations of $P^{R}_{2}N^{R'}_{2}$ ligands, and b) illustration of how the orientation of $P^{R}_{2}N^{R'}_{2}$ ligand can be influenced by attractive interactions between the lone pair on nitrogen and adjacent ligands.

The conformation and orientation of a $P^{R}_{2}N^{R'}_{2}$ ligand can be affected by the presence of attractive or repulsive interactions between the pendant amine and other ligands coordinated to the metal (Figure 1b). For example, pendant amines have been observed to adopt boat conformations to form attractive interactions with CO and isonitrile (CNR) ligands, which possess a partial positive charge on the C atoms.[28, 29] In contrast, pendant amines tend to adopt a chair conformation in order to avoid repulsive interactions with acetonitrile,[19, 30-35] chloride,[36] acetate,[19] and N_2 ligands.[37, 38] Some ligands, such as hydride or H_2, exhibit a delicate balance between an attractive or repulsive interaction with pendant amines. For example, the interaction between the pendant amine and a hydride ligand appears to be repulsive for $CpFe(P^{R}_{2}N^{R'}_{2})(H)$ complexes[29, 39, 40] and attractive for $[CpCo(P^{R}_{2}N^{R'}_{2})(H)]^{+}$ complexes.[41] Additionally, the solid state structure of $[CpFe(P^{Ph}_{2}N^{Bn}_{2})(H_2)]^{+}$ suggests a repulsive interaction between the pendant amine and the H_2 ligand, while DFT computations suggest these groups form a weak attractive interaction in solution.[29]

In this paper we report the synthesis and structural characterization of a series of octahedral Fe(II) complexes, $[Fe(P^{Ph}_{2}N^{Bn}_{2})_2(X)(Y)]^{n+}$, which are used to assess the conformational preferences of $P^{R}_{2}N^{R'}_{2}$ ligands as a function of the ligands X and Y (Figure 1b). Similar to the complexes described above, the $[Fe(P^{Ph}_{2}N^{Bn}_{2})_2(X)(Y)]^{n+}$ complexes reported in this work display a chair-boat conformation in the solid state. The pendant amine in the boat conformer will experience an attractive interaction with the adjacent X or Y ligand. The relative ordering of attractive and repulsive interactions between the pendant amines and ligands in the

first coordination sphere is determined by examining how the conformation of the $P^{Ph}{}_2N^{Bn}{}_2$ ligands change as the X and Y ligands are varied. Natural bond orbital (NBO) analysis is used to further understand the nature and strength of the different attractive and repulsive interactions.

Results

Synthesis and Structural Studies of *cis*-Fe($P^{Ph}{}_2N^{Bn}{}_2$)$_2$Cl$_2$, 1. The reaction of $FeCl_2$ with two equivalents of the $P^{Ph}{}_2N^{Bn}{}_2$ ligand results in nearly quantitative formation of *cis*-Fe($P^{Ph}{}_2N^{Bn}{}_2$)$_2$Cl$_2$, **1** (equation 1). The $^{31}P\{^1H\}$ NMR spectrum of the product shows two multiplets at 45.1 ppm and 31.8 ppm consistent with an AA'XX' spin system, and the ^1H NMR spectrum exhibits the resonances expected for phenyl and methylene resonances (see the Experimental section for detailed assignments, and Figures S1-S2 in the Electronic Supplementary Information (ESI)). Single crystals of **1** were grown by vapor diffusion of hexane into a fluorobenzene/toluene solution. An X-ray diffraction study (Figure 2) shows that the overall structure is that of a *cis*-octahedral complex with expected Fe-P and Fe-Cl distances, as shown by the values listed in Table S1.

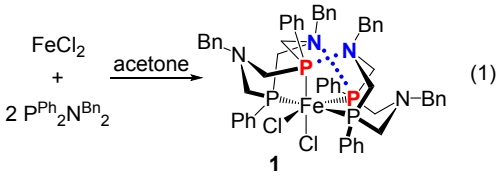

(1)

The six-membered ring of the $P^{Ph}{}_2N^{Bn}{}_2$ ligand adjacent to the chloride ligand adopts a chair conformation, which results in a large N-Cl distance of 3.819(2) Å. This ring conformation avoids the unfavorable electrostatic interactions between the lone pair of the pendant N atom and the partial negative charge on the chloride ligand. In contrast, the six-membered rings of the ligands that are adjacent to P atoms adopt boat conformations. The boat conformations place the pendant amines close to P atoms that are polarized to produce a partial positive charge. This geometry results in attractive interaction between nitrogen and phosphorus with N-P bond distances of 3.114(2) Å, significantly less than the van der Waals radius of 3.35 Å.[42, 43]

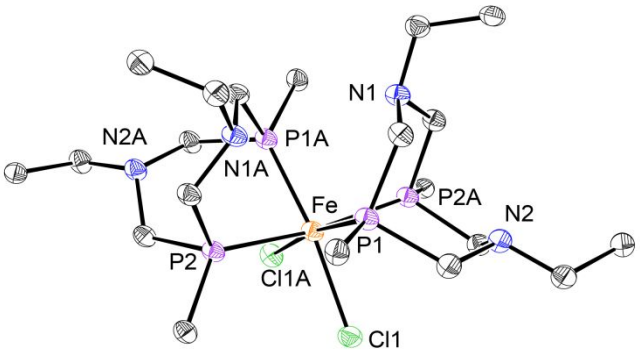

Figure 2. X-ray structural depiction of *cis*-Fe($P^{Ph}_2N^{Bn}_2$)$_2$Cl$_2$, **2**. The phenyl rings (other than the ipso carbon) and hydrogen atoms are omitted for clarity. Thermal ellipsoids are shown with 40% probability.

Synthesis and Characterization of [HFe($P^{Ph}_2N^{Bn}_2$)$_2$(CH_3CN)]BAr^F_4, 2. Purging a solution of the previously reported [Fe($P^{Ph}_2N^{Bn}_2$)$_2$(CH_3CN)$_2$](BF_4)$_2$ complex[44] with 1 atm of H_2 in the presence of *N*,*N*-diisopropylethylamine and one equivalent of $NaBAr^F_4$ (BAr^F = tetrakis[(3,5-trifluoromethyl)phenyl]borate) resulted in partial conversion to [HFe($P^{Ph}_2N^{Bn}_2$)$_2$(CH_3CN)]BAr^F_4 (equation 2). $NaBAr^F_4$ is used to increase the solubility of [Fe($P^{Ph}_2N^{Bn}_2$)$_2$(CH_3CN)$_2$]$^+$ in fluorobenzene, and the base deprotonates the intermediate dihydrogen complex. This reaction does not go to completion, because the displaced acetonitrile inhibits coordination of dihydrogen. However, this reaction can be driven to near completion by removing the acetonitrile produced during the reaction under vacuum, and repeating the entire procedure (adding base, H_2, and solvent, then removing solvent and acetonitrile) two more times. A $^{31}P\{^1H\}$ NMR spectrum recorded at 25 °C exhibits four doublet of doublets of doublets at 31.4, 50.4, 54.2, and 56.3 ppm that are assigned to *cis*-[HFe($P^{Ph}_2N^{Bn}_2$)$_2$(CH_3CN)]BAr^F_4, ***cis*-2**, and two broad peaks at 43 and 52 ppm, that are assigned to *trans*-[HFe($P^{Ph}_2N^{Bn}_2$)$_2$(CH_3CN)]BAr^F_4, ***trans*-2** (Figure S3). The two broad resonances for the trans isomer indicate that the phosphorus atoms exist in two different chemical environments. This arises from steric interactions between the phenyl substituents on phosphorus, which results in two P atoms closer to the hydride ligand and two closer to the acetonitrile ligand. As described in more detail below, *trans*-HFe($P^{Ph}_2N^{Bn}_2$)$_2$Cl (***trans*-3**) and *trans*-[HFe($P^{Ph}_2N^{Bn}_2$)$_2$(CO)]BAr^F_4 (***trans*-4**) exhibit similar spectral properties, and their structures are confirmed by high quality X-ray crystallographic structural determinations.

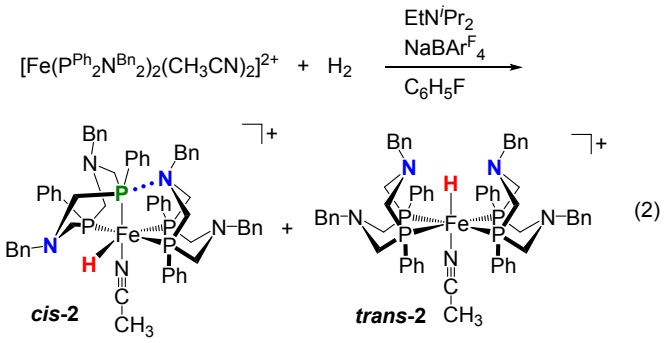

(2)

The ^{1}H NMR spectrum at -27 °C of the product mixture of ***cis-2*** and ***trans*-2** shows a hydride resonance at -9.61 ppm that appears as an overlapping doublet of quartets ($^{2}J_{PH}$ = 75.0, 35.0 Hz) (Figure S4). This resonance is assigned to the cis isomer for which the hydride ligand is coupled to the three roughly equivalent cis P atoms and to the trans P atom. A second hydride resonance appears as a triplet of triplets ($^{2}J_{PH}$ = 62.5, 30.0 Hz) at -18.66 ppm, and this resonance is assigned to the trans isomer. The triplet of triplets is expected for a hydride coupling to two different pairs of P atoms, one pair closer to the hydride ligand and one pair further away.

Single crystals of [HFe($P^{Ph}_2N^{Bn}_2$)$_2$(CH$_3$CN)]BAr$^F_4$ were grown by diffusion of hexane into a toluene solution of the product mixture. An X-ray diffraction study was carried out. Although the quality of the structure is not high, the data indicates that [HFe($P^{Ph}_2N^{Bn}_2$)$_2$(CH$_3$CN)]BAr$^F_4$ preferentially crystallizes as the trans isomer (Figure S22). The overall structure is analogous to that of the previously structurally characterized *trans*-[HFe($P^{Ph}_2N^{Ph}_2$)$_2$(CH$_3$CN)]BF$_4$ complex.[44] Although the data for ***trans*-2** reported here is not of sufficient quality to permit detailed metric comparisons, the basic structural features indicate that boat conformations are adopted by the two six-membered rings adjacent to the hydride ligand and two chair conformations for the two six-membered rings adjacent to acetonitrile. Computational analysis, discussed in detail below, revealed that the amine-hydride interaction is slightly repulsive because of a partial negative charge on the hydride ligand.

Synthesis and Structural Studies of *trans*-HFe($P^{Ph}_2N^{Bn}_2$)$_2$Cl, *trans*-3. The reaction of [HFe($P^{Ph}_2N^{Bn}_2$)$_2$(CH$_3$CN)]BAr$^F_4$ with excess Bu$_4$NCl in acetone gives the *trans*-HFe($P^{Ph}_2N^{Bn}_2$)$_2$Cl (***trans*-3**) as the exclusive product (equation 3). The ^{31}P{^{1}H} NMR spectrum at 25 °C in C$_6$D$_5$Cl shows two broad peaks at 47.9 ppm and 47.2 ppm, indicating that the phosphorus atoms have two distinct chemical environments (Figure S5). Upon cooling to -27 °C, the spectrum sharpens and becomes two complex multiplets, consistent with slowing an

exchange process. As for $[HFe(P^{Ph}_2N^{Bn}_2)_2(CH_3CN)]BAr^F_4$, the nonequivalence of the P atoms is attributed to a structural distortion resulting from steric interactions of the phosphine ligands, as confirmed by the structural studies discussed below. At 25 °C, the hydride resonance at -25.7 ppm is a quintet, consistent with coupling to four equivalent P atoms resulting from an exchange process that scrambles the four P atoms (Figures S6-S7). At -27 °C this resonance can be analyzed as an overlapping triplet of triplets ($^2J_{PH}$ = 63.5, 29.0 Hz), consistent with two different environments for the four P atoms in the slow exchange regime.

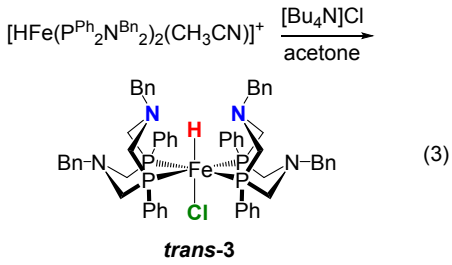

***trans*-3** (3)

Single crystals of ***trans*-3** were grown by vapor diffusion of hexane into a toluene solution of the complex. A drawing of this complex, resulting from an X-ray diffraction study, is shown in Figure 3, and selected bond distances and angles are given in Table S2. The structure is that of a severely distorted octahedral complex with the hydride and chloride ligands trans to each other. The hydride ligand was easily located in the difference Fourier map. The four P atoms are not in a plane as expected for an octahedral complex, and the dihedral angle between the two planes defined by two P atoms of each ligand and Fe, P(1)-Fe-P(2) and P(3)-Fe-P(4), is 24.5°. This twisting makes P(2) and P(3) closer to the hydride, and P(1) and P(4) closer to the chloride, consistent with the two broad peaks observed in the $^{31}P\{^1H\}$ NMR spectrum discussed above. Each $P^{Ph}_2N^{Bn}_2$ ligand in the structure displays a boat and a chair conformation. The two rings with the boat conformations are adjacent to the hydride ligand resulting in N•••H distances of 2.59 and 2.70 Å, compared to the sum of van der Waals radii of 2.75 Å.[42, 43] The two rings with the chair conformations are adjacent to the chloride ligand resulting in N•••Cl distances of 4.089(2) and 4.041(2) Å, compared to the sum of van der Waals radii of 3.30 Å.[42, 43] The preference for chair conformations of the rings adjacent to the chloride ligand arises from the repulsion of the partial negative charge of the chloride ligand with the lone pair of the pendant amine.

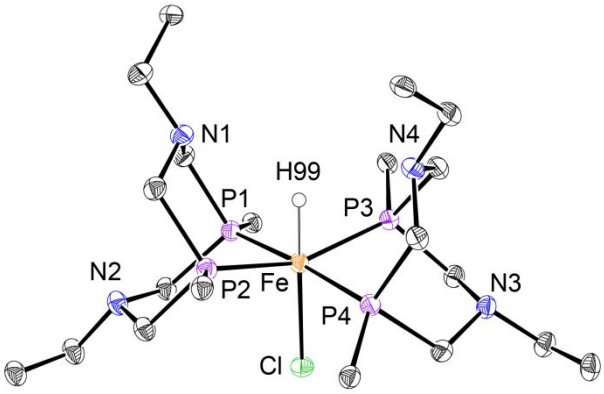

Figure 3. X-ray structural depiction of *trans*-HFe($P^{Ph}_2N^{Bn}_2$)$_2$Cl (***trans*-3**). The phenyl rings (other than the ipso carbon), and hydrogen atoms except for the hydride are omitted for clarity. Thermal ellipsoids are shown with 40% probability.

Synthesis and Structural Studies of *trans*-[HFe($P^{Ph}_2N^{Bn}_2$)$_2$(CO)]BAr^F_4, *trans*-4. The reaction of [HFe($P^{Ph}_2N^{Bn}_2$)$_2$(CH_3CN)]BAr^F_4 and CO in fluorobenzene results in the formation of *trans*-[HFe($P^{Ph}_2N^{Bn}_2$)$_2$(CO)]BAr^F_4, ***trans*-4** (equation 4). Again, due to the twisting of the two $P^R_2N^{R'}_2$ ligands with respect to each other, the $^{31}P\{^1H\}$ NMR spectrum of *trans*-[HFe($P^{Ph}_2N^{Bn}_2$)$_2$(CO)]BAr^F_4 in PhCl-d_5 at 25 °C shows two broad peaks at 50.6 ppm and 46.7 ppm, consistent with two different phosphorus environments (Figure S8, middle). Upon warming the sample to 80 °C these two resonances collapse to a singlet, and upon cooling to -27 °C a more resolved and complex spectrum consistent with an AA′XX′ spin system is observed (Figure S8). The hydride resonance at 25 °C (-8.10 ppm) is a triplet of triplets ($^2J_{PH}$ = 58.5, 27.5 Hz), consistent with coupling to two pairs of non-equivalent P atoms (Figure S10).

In addition to the trans isomer, ~8% of *cis*-[HFe($P^{Ph}_2N^{Bn}_2$)$_2$CO]BAr^F_4 (***cis*-4**) can be observed spectroscopically at all temperatures. The $^{31}P\{^1H\}$ NMR spectrum of the cis isomer in PhCl-d_5 at ambient temperature exhibits four doublets of doublets at 32, 37, 45, and 51 ppm, consistent with four different phosphorus environments (Figure S9). In addition, a hydride resonance is observed at -10.6 ppm in the ^1H NMR spectrum. This chemical shift is very similar to that observed for the hydride ligand of ***cis*-2** (-9.66), which is trans to a P atom. The chemical shift of the hydride ligands are sensitive to the identity of the ligand trans to it with values of -25.71 ppm for *trans*-HFe($P^{Ph}_2N^{Bn}_2$)$_2$Cl, -18.66 ppm for *trans*-[HFe($P^{Ph}_2N^{Bn}_2$)$_2$(CH_3CN)]BAr^F_4, -

12.66 ppm for *trans*-[HFe(H_2)($P^{Ph}_2N^{Bn}_2$)$_2$]BAr^F_4 (see below), and -8.10 ppm for *trans*-[HFe($P^{Ph}_2N^{Bn}_2$)$_2$(CO)]BAr^F_4.

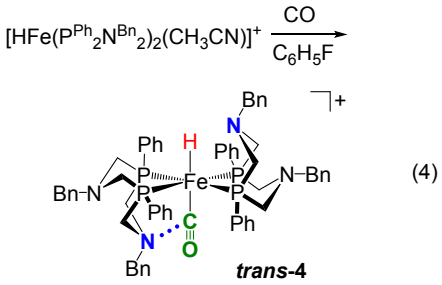

(4)

Single crystals of *trans*-[HFe($P^{Ph}_2N^{Bn}_2$)$_2$(CO)]BAr^F_4 were grown by layering a toluene solution of the complex with hexane. Figure 4 shows a drawing of the [HFe($P^{Ph}_2N^{Bn}_2$)$_2$(CO)]$^+$ cation resulting from an X-ray diffraction analysis of these crystals, and selected bond distances and angles are listed in Table S3. The structural solution confirms the presence of a hydride ligand trans to the CO ligand. The dihedral angle between plane P(1)-Fe(1)-P(2) and plane P(3)-Fe(1)-P(4) is 33.6°, even larger than that in *trans*-HFe($P^{Ph}_2N^{Bn}_2$)$_2$Cl. Each $P^{Ph}_2N^{Bn}_2$ ligand displays a boat and a chair conformation. The boat conformation adjacent to the hydride ligand results in an N(3)•••H(99) distance of 2.45 Å, and the boat conformation adjacent to the carbonyl ligand results in an N(2)••C(61) distance of 2.928(4) Å. Both distances are significantly less than the sum of the van der Waals radii, 2.75 and 3.25 Å, respectively.[42, 43] These distances suggest an attractive interaction between the N atoms of the boat conformations and the hydride ligand and the carbon atom of the carbonyl ligand. Computational analysis indicates that the N•••H interaction is repulsive in nature, while the N•••C interaction is weakly attractive.

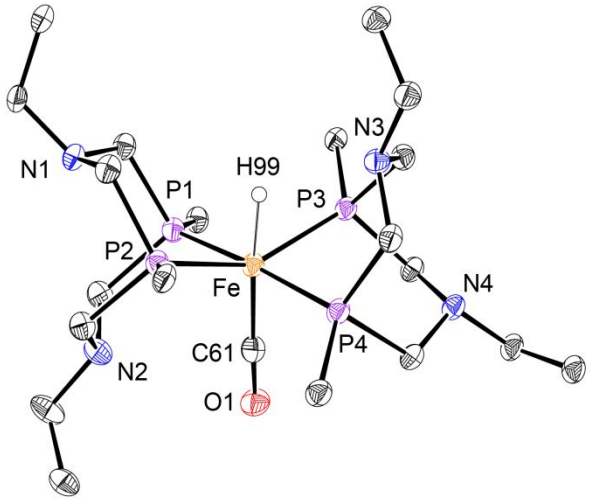

Figure 4. X-ray structural depiction of *trans*-[HFe($P^{Ph}_2N^{Bn}_2$)$_2$(CO)]BAr^F_4 (***trans*-4**). The anion, phenyl rings (other than the ipso carbon), and hydrogen atoms except for the hydride are omitted for clarity. Thermal ellipsoids are shown with 40% probability.

Protonation of *trans*-[HFe($P^{Ph}_2N^{Bn}_2$)$_2$(CO)]BAr^F_4. Reaction of one equivalent of 2,6-dichloroanilinium tetrakis(perfluorophenyl)borate with *trans*-[HFe($P^{Ph}_2N^{Bn}_2$)$_2$CO]BAr^F_4 in chlorobenzene at 80 °C resulted in a mixture of mono-protonated products (equation 5). At 80 °C the major product (approximately 80%) exhibits a singlet at 12.8 ppm and a quintet at -9.03 ppm in the ^{1}H NMR spectrum (Figures S11-S12). The singlet is assigned to a proton bridging the two pendant amines of a single diphosphine ligand, i.e. a pinched exo-protonated product (***trans*-5**). The quintet at -9.03 ppm is assigned to a hydride ligand that is coupled to four P atoms. At 80 °C, the ^{31}P{^{1}H} NMR spectrum exhibited two broad singlets at 46.3 ppm and 30.5 ppm, one of which is attributed to the phosphorus atoms of the protonated diphosphine ligand and the other is attributed to the phosphorus atoms of the non-protonated ligand (Figure S13). Upon cooling to -27 ˚C these two resonances show additional splitting, but a low temperature limiting spectrum is not observed. A ^{31}P-^{31}P COSY 2D experiment at -27 °C confirmed that these two resonances are coupled to each other (Figure S14).

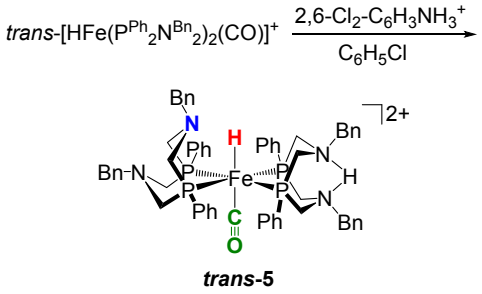

(5)

^{15}N-labeled [HFe($P^{Ph}_2N^{Bn}_2$)$_2$CO]BAr^F_4 was prepared in order to obtain further information on its protonated product. At 80 °C, the ^{15}N-H signal at 12.8 ppm in the ^{1}H NMR spectrum of the major isomer, ***trans*-5**, is a doublet of doublets with two different coupling constants, $^1J_{N(1)-H}$ = 46.5 Hz and $^1J_{N(2)-H}$ = 22.5 Hz (Figure S15). This spectrum is consistent with an exo-protonated pinched structure with the proton asymmetrically shared by the two nitrogen atoms. This interpretation is supported by ^{15}N{^{1}H} NMR spectra recorded at 80 °C, which exhibit four resonances at -327.3, -333.7, -336.0, and -339.1 ppm (Figure S16). The latter two resonances exhibit triplet patterns attributed to coupling to two P atoms of the same ligand. In addition, ^{15}N-^{1}H HSQC 2D NMR spectra recorded at 80 °C demonstrated that the proton signal at 12.8 ppm correlates with two different nitrogen atoms at -327.3 ppm and -333.1 ppm, respectively (Figure S17). Similar behavior has been reported in a previous protonation study of [HFe($P^{Ph}_2N^{Ph}_2$)$_2$(CH$_3$CN)]$^+$ that resulted in double exo-protonation,[44] in contrast to the mono-protonated product reported here.

The conformation of the non-protonated $P^{Ph}_2N^{Bn}_2$ ligand of ***trans*-5** could not be determined from the NMR spectra, and X-ray quality crystals of ***trans*-5** were not obtained. Assuming that the $P^{Ph}_2N^{Bn}_2$ ligand adopts a chair-boat conformation, the pendant amine of the ligand arm in a boat conformation could orient towards either the hydride ligand or the CO ligand. Computational analysis indicates that the former isomer, illustrated in equation 5, is the most stable conformation.

In addition to the dominant species ***trans*-5**, several additional products are observed in the ^{31}P{^{1}H} NMR spectrum upon protonation of *trans*-[HFe($P^{Ph}_2N^{Bn}_2$)$_2$CO]BAr^F_4. The second most abundant product exhibits a broad singlet (approximately 20% at 80 °C) at 48.83 ppm, and two broad resonances at 26.06 and 41.01 ppm are associated with a third very minor product

(Figure S13). These additional products likely correspond to other protonation isomers, but a definitive structural assignment could not be made from the available spectroscopic data.

Reaction of *trans*-HFe($P^{Ph}_2N^{Bn}_2$)$_2$Cl with H_2. Purging a chlorobenzene solution of *trans*-HFe($P^{Ph}_2N^{Bn}_2$)$_2$Cl and one equivalent of $NaBAr^F_4$ with H_2 results in nearly quantitative formation of *trans*-[HFe(H_2)($P^{Ph}_2N^{Bn}_2$)$_2$]BAr^F_4 (***trans*-6**, reaction 6). The ^{1}H NMR spectrum of this product at 25 °C exhibited two broad peaks at -7.57 ppm and -12.66 ppm, assigned to a dihydrogen ligand and a hydride ligand, respectively (Figure S18). Cooling the sample to -27 °C did not result in a resolved hydride resonance (Figure S19). A NOESY experiment performed at 25 °C with a mixing time of 25 ms indicated that the dihydrogen and hydride resonances were correlated, indicating exchange between these ligands (Figure S20). A similar exchange process has been reported for other *trans*-[HM(H_2)(diphosphine)$_2$]$^{2+}$ (M = Fe, Ru, Os) complexes.[45] The ^{31}P{^{1}H} NMR spectrum at 25 °C exhibited two broad peaks at 58.1 ppm and 54.0 ppm, consistent with a distorted trans geometry as discussed above for other trans complexes (Figure S21). Computational analysis indicates that the most stable isomer of ***trans*-6** has the amines in a boat conformation pointing towards the hydride ligand, as shown in equation 6.

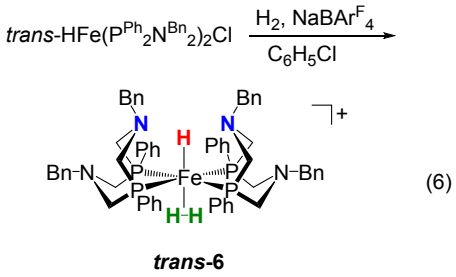

***trans*-6** (6)

Computational Analysis. More detailed insights into the conformational preferences of the $P^{Ph}_2N^{Bn}_2$ ligands in these complexes were obtained from electronic structural analysis. Density functional theory (DFT) was used to calculate the lowest energy conformations of complexes for which a solid-state structure was not obtained. Additionally, the NBO framework was used to calculate donor-acceptor interactions between the lone pair on the relevant pendant amines and the acceptor orbitals of the ligands bound to Fe. Given a donor orbital, D, and an acceptor orbital, A, the charge transferred between the orbitals, q_{CT}, can be estimated as a ratio

between the stabilization offered by the interaction of the two orbitals, $\Delta E_{DA}^{(2)}$, and the difference in orbital energies, $\varepsilon_A - \varepsilon_D$, according to equation 7.[46]

$$q_{CT} \cong \frac{|\Delta E_{DA}^{(2)}|}{\varepsilon_A - \varepsilon_D} \qquad (7)$$

For *cis*-Fe($P^{Ph}_2N^{Bn}_2$)$_2$Cl$_2$ (**1**), the geometry relaxes such that there are two N–P interactions, each *trans* from a Cl ligand. The N–P distances in both pairs are 3.05 Å, which is shorter than the distance of 3.11 Å observed in the solid state structure of **1**. There is a small amount of donation from the lone pair on the pendant amine to the P atom, leading to a stabilization energy ($\Delta E_{n\sigma^*}^{(2)}$) of 0.8 kcal/mol and a charge transfer (q_{CT}) of 0.001 Coulomb for each N-P pair. This interaction is quite weak, with about an order of magnitude less charge transfer than that seen in a typical hydrogen bond.

The complex *cis*-[HFe($P^{Ph}_2N^{Bn}_2$)$_2$(CH_3CN)]$^+$ (***cis*-2**) has a lower symmetry than **1**, the dichloride complex. As a result, the pendant amines can potentially interact with the hydride ligand or two different phosphine ligands. In the N–P pairs, the interactions are no longer symmetric, as one P is *trans* to the hydride ligand (P_H) and the other *trans* to CH_3CN (P_{CH3CN}). The calculated N–P_H and N–P_{CH3CN} distances are 3.04 and 3.06 Å, with stabilization energies of 1.3 and 0.9 kcal/mol respectively. Similarly, the charge transfers are not identical, with q_{CT}(N–P_H) and q_{CT}(N–P_{CH3CN}) values of 0.002 and 0.001. Though these interactions are quite weak, they are in agreement with the experimentally suggested attractor ordering of PR_3 > CH_3CN > Cl.

The interaction between the pendant amine and the hydride ligand is more complicated in both ***cis*-2** and ***trans*-2**. NBO analysis did not reveal the presence of a significant donor-acceptor interaction between the pendant amine and the hydride in either isomer. The geometries of the two complexes show an N–H distance of 2.51 Å in ***cis*-2** and distances of 2.47 and 2.58 Å in ***trans*-2**. The natural charges on the hydride ligands are -0.216 and -0.170, respectively, while the nitrogen atoms of the pendant amines carry charges between -0.467 and -0.476. These data suggest the amine-hydride interactions are slightly repulsive in nature, rather than favorable via donor-acceptor interactions. Similar results were obtained for *trans*-[HFe($P^{Ph}_2N^{Bn}_2$)$_2$(Cl) (***trans*-**

3), *trans*-[HFe($P^{Ph}_2N^{Bn}_2$)$_2$(CO)]$^+$ (***trans*-4**), and *trans*-[HFe($P^{Ph}_2N^{Bn}_2$)$_2$(H_2)]$^+$ (***trans*-6**), which indicates a systematic absence of an attractive N-H interaction within this family of complexes.

The protonated complex *exo-trans*-[HFe($P^{Ph}_2N^{Bn}_2$)($P^{Ph}_2N^{Bn}_2$H)(CO)] (***trans*-5**) was used to further understand the origin of the conformational preferences of complexes containing a hydride ligand. The *exo* protonation locks one of the $P^{Ph}_2N^{Bn}_2$ ligands in a chair-chair conformation away from the Fe center. As a result, the conformation of the remaining $P^{Ph}_2N^{Bn}_2$ can be systematically varied. The most stable isomer of ***trans*-5** does not possess an amine-carbonyl interaction. The second most stable isomer has an amine pointing towards both the hydride and carbonyl ligands (***trans*-5A**), while the highest energy isomer only shows an amine-carbonyl interaction (***trans*-5B**). Due to the positive charge carried on the carbon of the carbonyl ligand, one might suspect that the pendant amine would have a favorable donor-acceptor interaction with the carbonyl ligand. However, ***trans*-5A** and ***trans*-5B** show a very small stabilization energies of 0.5 kcal/mol for the amine-carbonyl interaction. The N•••C attractive interaction is even weaker for ***trans*-4** (< 0.5 kcal/mol), suggesting the interaction is stronger for complexes with a higher net charge.

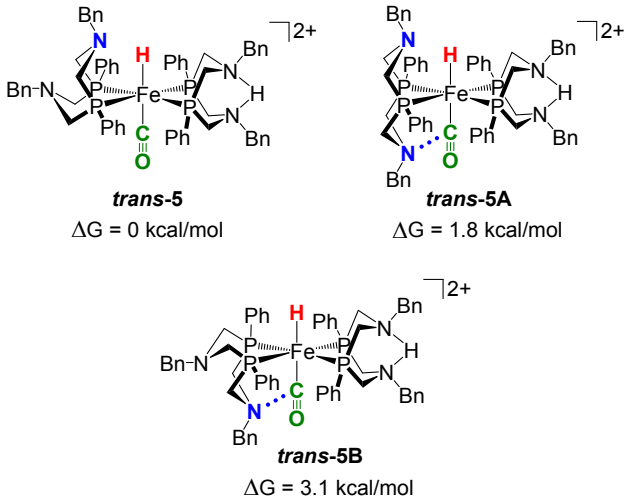

Figure 5. Relative free energies calculated for different conformations of ***trans*-5**.

These computational data indicate the complex is stabilized more by the non-bonding amine-hydride interaction than by the weakly attractive amine-carbonyl interaction. The relative stability of the isomers correlates roughly with the natural charge on the hydride and the carbon of the carbonyl, such that the relative energy increases with the negative charge on the hydride

and positive charge on the carbon (Table 1). The NBO analysis shows that formation of an amine-carbonyl interaction leads to an increase in the amount of charge transfer, q_{CT}(C→FeH), from the carbon atom of the carbonyl to the Fe–H antibonding orbital. Thus, the amine–carbonyl interaction shifts electron density from the carbon to the hydride, which destabilizes the complex.

Table 1. Relative free energy and select natural charges for the isomers of ***trans*-5**.

Isomer	ΔG_{rel} kcal/mol	q(C)	q(H)	q_{CT}(C→FeH)
***trans*-5**	0.0	0.099	-0.207	0.492
***trans*-5A**	1.8	0.137	-0.217	0.499
***trans*-5B**	3.1	0.146	-0.263	0.617

Analogous interactions are observed in the isomers of *trans*-$[HFe(H_2)(P^{Ph}_2N^{Bn}_2)_2]^{2+}$ (***trans*-6**). The lowest energy isomer (***trans*-6**) has an amine from each $P^{Ph}_2N^{Bn}_2$ ligand pointing towards the hydride ligand, along with a small negative charge on the hydride ligand (Figure 6). The isomers ***trans*-6A** and ***trans*-6B**, which have one or two amines pointing towards the H_2 ligand, are 4.6 and 4.5 kcal/mol higher in energy than ***trans*-6**. Hydrogen bonding interactions between H_2 and the pendant amine offer a stabilization energy, $\Delta E^{(2)}_{DA}$, of 5.5 kcal/mol, and are accompanied by a transfer of charge from the H_2 ligand to the hydride ligand, similar to the charge transfer displayed in the amine-carbonyl interaction (Table 2). The overall charge transfer is smaller within ***trans*-6A** and ***trans*-6B** than in ***trans*-6,** due in part to the increased distance between the iron center and the H_2 moiety (1.6 versus 2.0 Å).

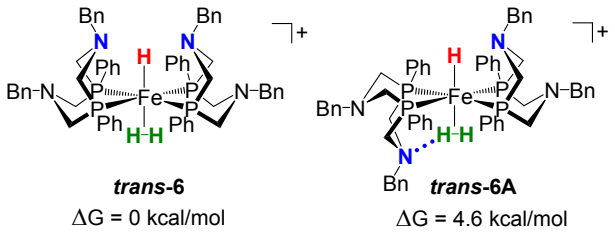

***trans*-6**
ΔG = 0 kcal/mol

***trans*-6A**
ΔG = 4.6 kcal/mol

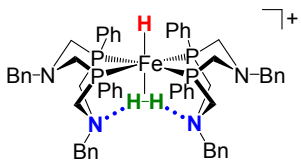

***trans*-6B**
ΔG = 4.5 kcal/mol

Figure 6. Relative free energies calculated for different conformations of ***trans*-6**.

Table 2. Relative free energy and select natural charges for the isomers of ***trans*-6**.

Isomer	ΔG_{rel} kcal/mol	$q(H_2)$	$q(H)$	$q_{CT}(H_2 \rightarrow FeH)$
***trans*-6**	0.0	-0.135	-0.123	0.101
***trans*-6A**	4.6	-0.067	-0.159	0.052
***trans*-6B**	4.5	-0.036	-0.229	0.057

Discussion

In this work, we investigated the conformational preferences of pendant amines in a series of $[Fe(P^{Ph}_2N^{Bn}_2)_2(X)(Y)]^{n+}$ complexes. Each pendant amine is part of a six-membered ring that can adopt either a chair or boat conformation. When the ring is in a boat conformation, the amine is positioned to interact with the other ligands (X or Y) that are coordinated to Fe. An "attractor order" can be defined as the relative ability of a particular ligand to attract a pendant amine in a boat conformation. The preference of a ligand to attract a pendant base in the second coordination sphere may contribute significantly to activation barriers for individual steps during electrocatalytic oxidation or production of H_2, such as H_2 binding, cleavage, and proton transfer.[27] Any of these steps can be rate-limiting, and decreasing the activation barriers by 2-4 kcal/mol can increase rates by 2-3 orders of magnitude.

For the $[Fe(P^{Ph}_2N^{Bn}_2)_2(X)(Y)]^{2+}$ complexes described in this work, the qualitative attractor order can be determined from observation of the ligand conformations in the solid-state structures and from calculation of the lowest energy conformations by DFT. The pendant amines adjacent to either chloride or acetonitrile ligands were always found to be in a chair conformation, indicating these ligands are very poor attractors. Formation of an N•••PR_3 interaction requires the complex to have a cis geometry. Only two species, **1** and ***cis*-2**, were observed to have a cis geometry, indicating that the phosphines of the $P^{Ph}_2N^{Bn}_2$ ligand are only very weak attractors for the pendant amines. The order of the remaining ligands can be assigned from the conformational analysis of ***trans*-5** and ***trans*-6** by DFT. The most stable conformation of these complexes is calculated to have both boat conformations adjacent to the hydride ligand, indicating that it is a strong attractor of the pendant amines. Placing the amine in a boat conformation adjacent to the CO ligand in ***trans*-5** or the H_2 ligand in ***trans*-6** destabilizes these

complexes by 3.1 kcal/mol and 4.5 kcal/mol, respectively, indicating that CO is a slightly better attractor than H_2. Together, these data suggest an attractor order of $H^- > CO > H_2 > PR_3 > Cl^- \sim CH_3CN$, where the conformation that places a pendant amine next to a hydride ligand is the most favorable.

The attractor ordering observed for $[Fe(P^{Ph}_2N^{Bn}_2)_2(X)(Y)]^{n+}$ does not correlate with the ability of the pendant amine to form a weak bond with the adjacent ligand. Based on NBO calculations, the strength of donor-acceptor interaction between the pendant amine decreases in the order $H_2 > PR_3 > CO > H^-$. The lack of a direct correlation between the attractor order and strength of the donor-acceptor interaction implies that multiple factors must be considered to predict the conformational preference of a pendant amine. One such factor is the steric profile of a given attractor ligand. For example, the pendant amine forms a slightly stronger electrostatic interaction with PR_3 (0.8-1.3 kcal/mol) of another $P^{Ph}_2N^{Bn}_2$ ligand than with CO (≤0.5 kcal/mol), yet PR_3 is a weaker overall attractor than CO, presumably due to its larger steric profile. A more subtle effect is observed for the hydride ligands, which appear to attract the pendant amines despite the absence of an amine-hydride donor-acceptor interaction. For example, in the most stable conformation of *trans*-$[HFe(H_2)(P^{Ph}_2N^{Bn}_2)_2]^{2+}$, each ligand adopts a conformation that places the pendant amine adjacent to the hydride ligand, even though the amines can form a strong hydrogen bond with the dihydrogen ligand (5.5 kcal/mol). NBO calculations revealed that formation of an N•••H_2 hydrogen bond leads to a net destabilization of the complex resulting from increased delocalization of electron density onto the hydride ligand.

A different attractor ordering can be assigned upon examination of previously reported complexes. Studies of *trans*-$[HMn(P^{Ph}_2N^{Bn}_2)(dmpm)(CO)]$ indicate that CO attracts the pendant amine more strongly than the hydride ligand.[47] Similarly, previous studies of $[CpFe(P^R_2N^{R'}_2)(H_2)]^+$, $CpFe(P^R_2N^{R'}_2)H$, and $[CpFe(P^R_2N^{R'}_2)(CO)]^+$ suggest that CO is a better attractor than H or H_2,[29] and the solid state structure of *cis*-$Cr(CO)_2(P^{Ph}_2N^{Bn}_2)_2$ suggests that PR_3 is a better attractor than CO.[37] These complexes suggest a tentative attractor ordering of $PR_3 > CO > H_2 \sim H^-$, which is substantially different from the ordering obtained from analysis of the $[Fe(P^{Ph}_2N^{Bn}_2)_2(X)(Y)]^{n+}$ complexes studied in this work. The difference in these orderings could reflect substantial electronic changes to the ligands upon changing the metal identity or the charge of the complex, or could result from the limited number of complexes available. Clearly

further work is needed to better assign a universal attractor ordering for any complex containing a $P^{R}{}_{2}N^{R'}{}_{2}$ ligand.

The observation of a short MH•••X contact between a metal hydride and a Lewis base is often taken as evidence of a hydrogen bond.[48, 49] In the complexes studied in this work, the pendant amine is positioned to form an intramolecular hydrogen bond with the hydride ligand, but a FeH•••N hydrogen bond does not exist due to the negative charge on the hydride ligand. Thus, additional evidence is needed to provide support for the presence of a MH•••X bond. In the case of intermolecular MH•••X bonds, IR spectroscopy and NMR spectroscopy have been used to observe the perturbation of the M-H bond upon addition of a base.[50-53] Spectroscopic detection of an intramolecular MH•••X bond is more challenging since the M-H bond cannot be observed in both the presence and absence of the hydrogen bond acceptor. In these cases, computational analysis provides a clear advantage over spectroscopic methods for analyzing the nature of the MH•••X interaction.

The discussions above focused on the interactions of pendant amines in the second coordination sphere with ligands in the first coordination sphere. However, during many catalytic cycles, the amine ligands in the second coordination sphere are protonated. In this case the rules governing attractive interactions between the positively charged protonated amines of second coordination sphere and ligands in the first coordination sphere will change dramatically. For protonated pendant amines, the competition with a second pendant amine, a ligand in the first coordination sphere, or the metal center (particularly for low oxidation states) will determine the thermodynamically most stable structure. For *trans*-$[HFe(P^{Ph}{}_{2}N^{Bn}{}_{2})(P^{Ph}{}_{2}N^{Bn}{}_{2}H)(CO)]^{2+}$, the exo-protonated structure is the most stable isomer. However, for low valent nickel complexes reported previously, endo-protonated species in which the NH proton interacts directly with a Ni(I) or Ni(0) center are of comparable energy.[54-58] The relative ordering of conformational preferences in protonated complexes remains to be determined. However, it is different from the ordering reported here for unprotonated complexes.

Conclusions

Structural studies of $[Fe(P^{Ph}{}_{2}N^{Bn}{}_{2})_{2}(X)(Y)]^{n+}$ complexes suggest a ligand attractor ordering of $H^{-} > CO > H_{2} > PR_{3} > Cl^{-} \sim CH_{3}CN$, with H^{-} exerting the greatest attraction for pendant amine bases in the second coordination sphere. For electrocatalytic cycles, such

preferences may contribute significantly to activation barriers for key reactions such as H_2 binding, cleavage, or proton transfer. In addition, protonation of pendant amines in the second coordination sphere leads to different conformational preferences compared to unprotonated complexes. For example, both $P^{Ph}_2N^{Bn}_2$ ligands of *trans*-$[HFe(P^{Ph}_2N^{Bn}_2)_2(CO)]^+$ adopt boat/chair conformations, whereas the protonated $P^{Ph}_2N^{Bn}_2$ ligand of *trans*-$[HFe(P^{Ph}_2N^{Bn}_2)(P^{Ph}_2N^{Bn}_2H)(CO)]^{2+}$ adopts a chair/chair conformation, enabling the proton to be shared between the two N atoms of the diphosphine ligand. Protonation/deprotonation reactions will often be accompanied by conformational changes, adding another important consideration to catalyst design. The interactions between ligands in the first coordination sphere and functional groups in the second coordination sphere need to be fully understood to design redox catalysts with performances rivaling those of enzymes.

Experimental

General Methods. ^{1}H NMR, $^{31}P\{^1H\}$ NMR, and $^{15}N\{^1H\}$ NMR spectra were recorded on a Varian 500 MHz NMR spectrometer. $^{31}P\{^1H\}$ NMR spectra are referenced to a phosphoric acid external standard. ^{1}H chemical shifts are referenced to TMS using known values of residual solvent proton shifts.[59] $^{15}N\{^1H\}$ chemical shifts are reported relative to CH_3NO_2.

Synthesis of Ligands and Complexes and Sources of Materials. All reactions were performed under an argon atmosphere in a glove box. Solvents were dried using standard procedures and degassed under argon. Deuterated NMR solvents were degassed using the freeze-pump-thaw method. Sodium tetrakis(3,5-bis(trifluoromethyl)phenyl)borate, potassium tetrakis(perfluorophenyl)borate, 2,6-dichloroaniline, $HBF_4\cdot(C_2H_5)_2O$, and anhydrous $FeCl_2$ were obtained from commercial sources and used without further purification. $[Fe(CH_3CN)_6](BF_4)_2$[60, 61] and $P^{Ph}_2N^{Bn}_2$[62] were prepared as previously described.

***cis*-$[Fe(P^{Ph}_2N^{Bn}_2)_2(CH_3CN)_2](BF_4)_2$**: CH_2Cl_2 (10 mL) was added to a mixture of $[Fe(CH_3CN)_6](BF_4)_2$ (238 mg, 0.500 mmol) and $P^{Ph}_2N^{Bn}_2$ (483 mg, 1.00 mmol). The suspension was stirred overnight at room temperature. The resulting orange suspension was filtered to remove trace amounts of solids, and the solvent was removed from the filtrate by applying a vacuum. The orange powder that was obtained was washed with ether (10 mL × 3). Yield: 606 mg, 0.475 mmol, 95%. The $^{31}P\{^1H\}$ NMR and ^{1}H NMR spectra matched previously published data.[44]

***cis*-Fe($P^{Ph}_2N^{Bn}_2$)$_2Cl_2$**: Acetone (50 mL) was added to a mixture of $FeCl_2$ (63 mg, 0.500 mmol) and $P^{Ph}_2N^{Bn}_2$ (483 mg, 1.00 mmol). The purple solution was stirred at room temperature overnight, and the solvent was evaporated. The resulting purple powder was washed with hexane (15 mL × 3). Yield: 518 mg, 0.475 mmol, 95%. Crystals suitable for X-ray diffraction studies were grown by vapor diffusion of hexane into a fluorobenzene/toluene solution. Anal. Calc. for $C_{60}H_{64}Cl_2FeN_4P_4 \cdot PhF$: C, 66.73; H, 5.85; N, 4.72. Found: C, 66.88; H, 5.98; N, 4.72. $^{31}P\{^1H\}$ NMR (Fe($P^{Ph}_2N^{Bn}_2$)$_2Cl_2 \cdot C_6H_5F$ in C_6D_5Cl, 25 °C, ppm): 45.6-44.7 (m, P trans to Cl), 32.2-31.3 (m, P trans to P). ^1H NMR (Fe($P^{Ph}_2N^{Bn}_2$)$_2Cl_2 \cdot C_6H_5F$, C_6D_5Cl, 25 °C, ppm): 8.07 (br, 4H, C_6H_5), 7.89 (s, 2H, C_6H_5), 7.43-7.37 (m, 4H, C_6H_5), 7.32-7.26 (m, 10H, C_6H_5), 7.24-7.20 (m, 3H, C_6H_5), 7.17-7.10 (m, 6H, C_6H_5), 6.45 (d, ^3J = 7.1 Hz, 4H, C_6H_5), 4.53 (d, ^2J = 11.1 Hz, 2H, PhCH_2N), 3.89 (d, ^2J = 11.1 Hz, 2H, PhCH_2N), 3.71 (d, ^2J = 13.6 Hz, 2H, CH_2N), 3.36 (d, ^2J = 13.4 Hz, 2H, CH_2N), 3.23-3.18 (m, 4H, CH_2N), 3.01-2.93 (m, 6H, CH_2N), 2.56 (d, ^2J = 10.7 Hz, 2H, CH_2N), 2.33-2.29 (m, 2H, CH_2N), 1.66-1.62 (m, 2H, CH_2N).

[HFe($P^{Ph}_2N^{Bn}_2$)$_2$(CH_3CN)]BAr^F_4: A one to one ratio of [Fe($P^{Ph}_2N^{Bn}_2$)$_2$(CH_3CN)$_2$](BF_4)$_2$ (255 mg, 0.200 mmol) and $NaBAr^F_4$ (177 mg, 0.200 mmol) was dissolved in C_6H_5F (30 mL) and stirred for 1 h. Hünig's base (diisopropylethylamine, 68 μL, 0.40 mmol) was added to the solution followed by a 15-minute hydrogen purge. The flask was sealed, and the reaction mixture stirred overnight. After removing all the solvent with a vacuum, C_6H_5F (30 mL), Hünig's base (68 μL, 0.4 mmol), and hydrogen were added again, and the mixture was stirred overnight. This procedure was repeated a third time. After removing the solvent by applying a vacuum, the residue was washed with hexane (20 mL×3). Toluene (20 mL) was added to the powder that remained, and the suspension stirred overnight. The precipitate that remained was collected by filtration, washed with hexane (20 mL×3), and dried in a vacuum. Yield: 289 mg, 0.150 mmol 75%. Anal. Calc. for $C_{94}H_{80}BF_{24}FeN_5P_4 \cdot C_6H_5Me$: C, 60.10; H, 4.39; N, 3.47. Found: C, 59.41; H, 4.57; N, 3.60. $^{31}P\{^1H\}$ NMR (C_6H_5F, 25 °C, ppm): 56.7 (ddd, $^2J_{PP}$ = 113 Hz, $^2J_{PP}$ = 65 Hz, $^2J_{PP}$ = 26 Hz, *cis*-hydride), 54.5 (ddd, $^2J_{PP}$ = 79 Hz, $^2J_{PP}$ = 66 Hz, $^2J_{PP}$ = 63 Hz, *cis*-hydride), 52.0 (br, *trans*-hydride), 50.4 (ddd, $^2J_{PP}$ = 111 Hz, $^2J_{PP}$ = 67 Hz, $^2J_{PP}$ = 44 Hz, *cis*-hydride), 43.2 (br, *trans*-hydride), 31.7 (ddd, $^2J_{PP}$ = 79 Hz , $^2J_{PP}$ = 45 Hz, $^2J_{PP}$ = 28 Hz, *cis*-hydride). ^1H NMR (C_6D_5Cl, -27 °C, ppm): 8.53 (s, 8H, B($C_8F_6H_3$)$_4$), 7.66 (s, 4H, B($C_8F_6H_3$)$_4$), 7.58-7.27 (m), 7.17-6.94 (m), 6.84-6.80 (m), 6.66 (m), 6.57-6.51 (m) (40 H total, C_6H_5), 4.19-4.06 (m), 3.97-3.91 (m), 3.68-3.56 (m), 3.43-3.22 (m), 3.13-2.95 (m), 2.87-2.81 (m), 2.74 (br), 2.59 (br), 2.49 (br),

2.36 (m), 2.29-2.24 (m), 2.02-1.98 (m) (27 H total), -9.61 (qd, $^2J_{PH}$ = 75.0 Hz, $^2J_{PH}$ = 35.0 Hz, 0.57H, *cis*-Fe-*H*), -18.66 (tt, $^2J_{PH}$ = 62.5 Hz, $^2J_{PH}$ = 30.0 Hz, 0.43H, *trans*-Fe-*H*).

***trans*-HFe($P^{Ph}_2N^{Bn}_2$)$_2$Cl**: Acetone (10 mL) was added to a mixture of [HFe($P^{Ph}_2N^{Bn}_2$)$_2$(CH_3CN)]BAr^F_4 (385 mg, 0.20 mmol) and Bu_4NCl (278 mg, 1.0 mmol). The resulting red mixture was stirred for 1 h at room temperature and filtered to remove a small amount of white precipitate. The solvent was removed from the filtrate with a vacuum to produce a red solid. This solid was extracted with toluene, and the volume of the toluene extract was reduced to approximately 2 mL by applying a vacuum. Red crystals were obtained upon vapor diffusion of hexane into the toluene solution. They were collected by filtration, washed with toluene/hexane (1/1), and dried in a vacuum. Yield: 92 mg, 0.080 mmol, 40%. Crystals suitable for X-ray diffraction studies were grown by vapor diffusion of hexane into a toluene solution. Anal. Calc. for $C_{60}H_{65}ClFeN_4P_4$·PhMe: C, 70.00; H, 6.40; N, 4.87. Found: C, 70.14; H, 6.44; N, 4.82. $^{31}P\{^1H\}$ NMR (toluene-d_8, 25 °C, ppm): 47.9 (br), 47.2 (br). ^1H NMR (HFe($P^{Ph}_2N^{Bn}_2$)$_2$Cl·C_6H_5Me in toluene-d_8, -27 °C, ppm): 7.74 (br, 4H, C_6H_5), 7.44 (d, ^3J = 7.4 Hz, 4H, C_6H_5), 7.31 (t, ^3J = 7.6 Hz, 4H, C_6H_5), 7.24-7.19 (m), 7.15-7.10 (m), 7.07-7.04 (m), 6.99-6.98 (m) (22 H total, C_6H_5), 6.87-6.81 (m, 6H, C_6H_5), 6.62 (t, ^3J = 7.2 Hz, 2H, C_6H_5), 6.46 (t, ^3J = 7.1 Hz, 4H, C_6H_5), 4.32 (d, ^2J = 11.3 Hz, 2H, PhCH_2N), 4.04-4.00 (m, 4H, CH_2N), 3.98-3.91 (m, 2H, CH_2N), 3.44 (d, ^2J = 12.7 Hz, 2H, CH_2N), 3.30 (d, ^2J = 12.7 Hz, 2H, CH_2N), 3.23 (d, ^2J = 11.2 Hz, 4H, CH_2N), 3.02 (br, 4H, CH_2N), 2.83 (d, ^2J = 10.8 Hz, 2H, CH_2N), 2.24 (br, 2H, CH_2N), 2.11 (s, 3H, CH_3), -25.71 (tt, $^2J_{PH}$ = 63.5 Hz, $^2J_{PH}$ = 29.0 Hz, 1H, Fe-*H*).

***trans*-[HFe($P^{Ph}_2N^{Bn}_2$)$_2$(CO)]BAr^F_4**: CO was bubbled into a solution of [HFe($P^{Ph}_2N^{Bn}_2$)$_2$(CH_3CN)]BAr^F_4] (0.192 g, 0.100 mmol) in fluorobenzene (10 mL) for 20 min, the vial was closed, and the solution stirred overnight. Fluorobenzene was removed under vacuum, and the residue was dissolved in ether (2 mL). Hexane (20 mL) was layered on top. The resulting colorless crystals were collected by filtration and washed with hexane (12 mL × 3). Yield: 143 mg, 0.075 mmol, 75%. Crystals suitable for X-ray diffraction studies were grown by layering hexane onto a toluene solution followed by diffusion. Anal. Calc. for $C_{93}H_{77}BF_{24}FeN_4OP_4$: C, 58.39; H, 4.06; N, 2.93. Found: C, 58.10; H, 4.08; N, 2.99. $^{31}P\{^1H\}$ NMR (C_6D_5Cl, 25 °C, ppm): 50.6 (br), 46.7 (br). ^1H NMR (C_6D_5Cl, -27 °C, ppm): 8.39 (s, 8H, B($C_8F_6H_3$)$_4$), 7.53 (s, 4H, B($C_8F_6H_3$)$_4$), 7.36-7.18 (m), 7.18-7.15 (m), 6.85-6.77 (m), 6.76-6.73 (m), 6.54 (br) (40 H total, C_6H_5), 3.94 (d, ^2J = 12.8 Hz, 2H, PhCH_2N), 3.83 (d, ^2J = 13.0 Hz, 2H,

CH_2N), 3.53 (d, ^2J = 11.7 Hz, 2H, CH_2N), 3.29 (d, ^2J = 12.5 Hz, 2H, CH_2N), 3.06 (d, ^2J = 11.4 Hz, 2H, CH_2N), 2.92-2.75 (m, 12H, CH_2N), 2.66-2.57 (m, 2H, CH_2N), -8.21 (tt, $^2J_{PH}$ = 58.5 Hz, $^2J_{PH}$ = 27.5, 1H, Fe-*H*).

Protonation of [HFe($P^{Ph}_2N^{Bn}_2$)$_2$(CO)]BAr^F_4. 2,6-Dichloroanilinium tetrakis(perfluorophenyl)borate (8.4 mg, 0.010 mmol), [HFe($P_2^{Ph}N_2^{Bn}$)$_2$(CO)]BAr^F_4 (19.1 mg, 0.010 mmol), and C_6D_5Cl were added to an NMR tube. The tube was shaken for 30 s. then heated to 80 °C overnight. $^{31}P\{^1H\}$ NMR (C_6D_5Cl, 80 °C, ppm): Major product (76%), 46.3 (br s), 30.5 (br s). $^{31}P^{31}P$ COSY (80 °C) confirmed coupling between two resonances assigned to major product. Minor products, 48.8 (br s, 20%), 41.8 (br s, 1%), 41.0 (s, 1%), 26.06 (br s, 2%). ^1H NMR (C_6D_5Cl, 80 °C, ppm): major product (83%), 12.80 (s, N-*H*), -9.03 (quintet, $^2J_{PH}$ = 47.4 Hz, Fe-*H*); minor product (17%), -8.26 (quintet, $^2J_{PH}$ = 47.4 Hz, Fe-*H*) .

Protonation of ^{15}N-labeled [HFe($P^{Ph}_2N^{Bn}_2$)$_2$(CO)]BAr^F_4. ^{15}N-labeled [HFe($P^{Ph}_2N^{Bn}_2$)$_2$(CO)]BAr^F_4 was synthesized using an ^{15}N-labeled $P^{Ph}_2N^{Bn}_2$ ligand. Protonation was performed under the same conditions as described for the unlabeled [HFe($P^{Ph}_2N^{Bn}_2$)$_2$(CO)]BAr^F_4. ^1H NMR (C_6D_5Cl, ^{15}N-coupled, 80 °C, ppm): major product: 12.80 (dd, $^1J_{NH}$ = 46.5 Hz, $^1J_{NH}$ = 22.5 Hz, N-*H*), -9.03 (quintet, $^2J_{PH}$ = 47.4 Hz, Fe-*H*). $^{15}N\{^1H\}$ NMR, 80 °C, ppm): major product, -327.3 (d), -333.0 (br s), -336.5 (t), -338.1 (t). ^{15}N-^{1}H HSQC experiment was also performed at 80 °C. Nitrogen atoms with chemical shifts at -327.3 ppm and -333.0 ppm have correlations to the N-H resonances at 12.80.

Reaction of *trans*-HFe($P^{Ph}_2N^{Bn}_2$)$_2$Cl with H_2. HFe($P^{Ph}_2N^{Bn}_2$)$_2$Cl (10.6 mg, 0.010 mmol) and $NaBAr^F_4$ (8.8 mg 0.010 mmol) were dissolved in C_6D_5Cl in an NMR tube, and the resulting solution was purged with hydrogen for 10 min producing a color change from red to pale yellow. $^{31}P\{^1H\}$ NMR (C_6D_5Cl, 25 °C, ppm): 58.1 (br), 54.0 (br). ^1H NMR (C_6D_5Cl, 25 °C, ppm): -7.57 (br, 2H, Fe-(H_2)), -12.66 (br, 1H, Fe-*H*). A NOESY experiment with the mixing time of 25 ms showed that the peaks at -7.57 ppm and -12.66 ppm are correlated.

Single crystal X-ray structural analysis. Single crystals were coated in Paratone-N oil, mounted on a Siemens SMART diffractometer on a glass fiber under a stream of N_2 cooled to 110 K. All data were collected using a Mo Kα radiation source and a graphite monochromator. The data were collected, integrated, and corrected for absorption effects with the APEX II software package.[63] The structures were solved using direct methods and refined by least-squares methods on F^2 using the SHELXTL software package.[64] Thermal parameters for all non-

hydrogen atoms were refined anisotropically, unless otherwise noted. Hydrogen atoms except the hydrides for *trans*-HFe($P^{Ph}_2N^{Bn}_2$)$_2$Cl and *trans*-[HFe($P^{Ph}_2N^{Bn}_2$)$_2$CO]BAr^F_4 were added at the ideal positions and refined using a riding model where the thermal parameters were set at 1.2 times those of the attached carbon (1.5 times for methyl carbons). The hydride for *trans*-HFe($P^{Ph}_2N^{Bn}_2$)$_2$Cl and *trans*-[HFe($P^{Ph}_2N^{Bn}_2$)$_2$CO]BAr^F_4 were located in the difference Fourier map and refined isotropically.

The fluorine atom of the cocrystallized fluorobenzene molecule in the structure for *cis*-Fe($P^{Ph}_2N^{Bn}_2$)$_2$Cl$_2$ was constrained to 50% occupancy since the solvent molecule resides on a mirror plane. This solvent molecule was modeled as fluorobenzene since there is no apparent toluene in the ^{1}H NMR of the material. The structure of *trans*-HFe($P^{Ph}_2N^{Bn}_2$)$_2$Cl displays positional disorder of one of the phenyl groups on the pendant amine. This disorder was modeled using a two site model using the PART command and the disordered atoms were refined anisotropically. The structure of *trans*-[HFe($P^{Ph}_2N^{Bn}_2$)$_2$CO]BAr^F_4 displays positional disorder of three of the CF_3 groups of the BAr^F_4 anion. This disorder was modeled using a two site model using the PART command, assigning a different free variable for each CF_3 group and the disordered atoms were refined anisotropically. The C-F distances of the disordered CF_3 groups were restrained using the DFIX command to ensure reasonable bond lengths.

Computational Methods. The geometries of relevant complexes were calculated using the BP86 functional[65-67] incorporating dispersion effects with the Becke-Johnson damped D3 correction.[68, 69] The 6-31G** basis set[70, 71] was used on all atoms with the Stuttgart-Dresden ECP used on Fe.[72] Reported free energies include frequency calculations used to determine finite temperature effects at 298.15 K and zero-point vibrational energies. Single point calculations at the same level of theory were used to determine solvation effects in chlorobenzene using the SMD model.[73] All calculations were completed in ORCA 4.0.[74] This method has been previously successful for modeling metal vs. ligand protonation and hydrogen bonding interactions.[75, 76] NBO analysis was calculated using NBO 6.0[77] and wavefunctions calculated with the 6-31G basis set.[71]

Conflicts of Interest.

There are no conflicts to declare.

Electronic Supplemenatary Information (ESI) available: NMR spectra and tables of bond lengths and bond angles from X-ray analysis (pdf), computational details (pdf), computed molecule Cartesian coordinates (xyz), X-ray crystallographic data (cif, CCDC 1860782-1860784). See DOI: 10.1039/x0xx00000x.

Acknowledgments

This work was supported by the Center for Molecular Electrocatalysis, an Energy Frontier Research Center funded by the U.S. Department of Energy, Office of Science, Office of Basic Energy Sciences. Pacific Northwest National Laboratory (PNNL) is operated by Battelle for the U.S. DOE. Computations were performed using the Cascade supercomputer at the Environmental Molecular Sciences Laboratory, a National Scientific User Facility sponsored by the DOE's Office of Biological and Environmental Research and located at PNNL. We thank Dr. Mary Rakowski DuBois for helpful discussions.

References

1. C. J. Curtis, A. Miedaner, R. Ciancanelli, W. W. Ellis, B. C. Noll, M. Rakowski DuBois and D. L. DuBois, *Inorg. Chem.*, 2003, **42**, 216-227.
2. A. D. Wilson, R. H. Newell, M. J. McNevin, J. T. Muckerman, M. Rakowski DuBois and D. L. DuBois, *J. Am. Chem. Soc.*, 2006, **128**, 358-366.
3. M. Rakowski DuBois and D. L. DuBois, *Chem. Soc. Rev.*, 2009, **38**, 62-72.
4. D. L. DuBois, *Inorg. Chem.*, 2014, **53**, 3935-3960.
5. R. M. Bullock and M. L. Helm, *Acc. Chem. Res.*, 2015, **48**, 2017-2026.
6. A. Dutta, A. M. Appel and W. J. Shaw, *Nat. Rev. Chem.*, 2018, **2**, 244-252.
7. C. M. Klug, A. Cardenas, R. M. Bullock, M. O'Hagan and E. S. Wiedner, *ACS Catal.*, 2018, **8**, 3286-3296.
8. C. N. Virca, J. R. Lohmolder, J. B. Tsang, M. M. Davis and T. M. McCormick, *J. Phys. Chem. A*, 2018, **122**, 3057-3065.
9. R. L. Shook and A. S. Borovik, *Inorg. Chem.*, 2010, **49**, 3646-3660.
10. D. K. Dogutan, R. McGuire and D. G. Nocera, *J. Am. Chem. Soc.*, 2011, **133**, 9178-9180.
11. S. Bhunia, A. Rana, P. Roy, D. J. Martin, M. L. Pegis, B. Roy and A. Dey, *J. Am. Chem. Soc.*, 2018, **140**, 9444-9457.

12. W. A. Hoffert, M. T. Mock, A. M. Appel and J. Y. Yang, *Eur. J. Inorg. Chem.*, 2013, **2013**, 3846-3857.
13. B. D. Steffey, C. J. Curtis and D. L. DuBois, *Organometallics*, 1995, **14**, 4937-4943.
14. A. M. Herring, B. D. Steffey, A. Miedaner, S. A. Wander and D. L. DuBois, *Inorg. Chem.*, 1995, **34**, 1100-1109.
15. I. Azcarate, C. Costentin, M. Robert and J.-M. Savéant, *J. Am. Chem. Soc.*, 2016, **138**, 16639-16644.
16. C. Costentin, S. Drouet, M. Robert and J. M. Savéant, *Science*, 2012, **338**, 90-94.
17. Eva M. Nichols, J. S. Derrick, S. K. Nistanaki, P. T. Smith and C. J. Chang, *Chem. Sci.*, 2018, **9**, 2952-2960.
18. A. Chapovetsky, M. Welborn, J. M. Luna, R. Haiges, T. F. Miller and S. C. Marinescu, *ACS Cent. Sci.*, 2018, **4**, 397-404.
19. B. R. Galan, J. Schöffel, J. C. Linehan, C. Seu, A. M. Appel, J. A. S. Roberts, M. L. Helm, U. J. Kilgore, J. Y. Yang, D. L. DuBois and C. P. Kubiak, *J. Am. Chem. Soc.*, 2011, **133**, 12767-12779.
20. C. S. Seu, A. M. Appel, M. D. Doud, D. L. DuBois and C. P. Kubiak, *Energy Environ. Sci.*, 2012, **5**, 6480-6490.
21. C. J. Weiss, E. S. Wiedner, J. A. S. Roberts and A. M. Appel, *Chem. Commun.*, 2015, **51**, 6172-6174.
22. C. J. Weiss, P. Das, D. L. Miller, M. L. Helm and A. M. Appel, *ACS Catal.*, 2014, **4**, 2951-2958.
23. E. W. Dahl, T. Louis-Goff and N. K. Szymczak, *Chem. Commun.*, 2017, **53**, 2287-2289.
24. C. L. Ford, Y. J. Park, E. M. Matson, Z. Gordon and A. R. Fout, *Science*, 2016, **354**, 741-743.
25. C. M. Moore and N. K. Szymczak, *Chem. Sci.*, 2015, **6**, 3373-3377.
26. An analysis of the Cambridge Crystallographic Database (January 2019) revealed 184 structures of transition metal complexes containing a $P^R{}_2N^{R'}{}_2$ ligand. These structures displayed chair-boat (163), boat-boat (17), chair-chair (3), and distorted (1) conformations.
27. S. Raugei, S. T. Chen, M. H. Ho, B. Ginovska-Pangovska, R. J. Rousseau, M. Dupuis, D. L. DuBois and R. M. Bullock, *Chem. Eur. J.*, 2012, **18**, 6493-6506.

28. A. D. Wilson, K. Fraze, B. Twamley, S. M. Miller, D. L. DuBois and M. Rakowski DuBois, *J. Am. Chem. Soc.*, 2008, **130**, 1061-1068.
29. T. Liu, S. Chen, M. J. O'Hagan, M. Rakowski DuBois, R. M. Bullock and D. L. DuBois, *J. Am. Chem. Soc.*, 2012, **134**, 6257-6272.
30. U. J. Kilgore, M. P. Stewart, M. L. Helm, W. G. Dougherty, W. S. Kassel, M. Rakowski DuBois, D. L. DuBois and R. M. Bullock, *Inorg. Chem.*, 2011, **50**, 10908-10918.
31. W. A. Hoffert, J. A. S. Roberts, R. M. Bullock and M. L. Helm, *Chem. Commun.*, 2013, **49**, 7767-7769.
32. A. Jain, S. Lense, J. C. Linehan, S. Raugei, H. Cho, D. L. DuBois and W. J. Shaw, *Inorg. Chem.*, 2011, **50**, 4073-4085.
33. A. Jain, M. L. Reback, M. L. Lindstrom, C. E. Thogerson, M. L. Helm, A. M. Appel and W. J. Shaw, *Inorg. Chem.*, 2012, **51**, 6592-6602.
34. E. S. Wiedner, J. Y. Yang, W. G. Dougherty, W. S. Kassel, R. M. Bullock, M. Rakowski DuBois and D. L. DuBois, *Organometallics*, 2010, **29**, 5390-5401.
35. C. M. Klug, W. G. Dougherty, W. S. Kassel and E. S. Wiedner, *Organometallics*, 2018.
36. J. A. Franz, M. O'Hagan, M.-H. Ho, T. Liu, M. L. Helm, S. Lense, D. L. DuBois, W. J. Shaw, A. M. Appel, S. Raugei and R. M. Bullock, *Organometallics*, 2013, **32**, 7034-7042.
37. M. T. Mock, S. T. Chen, R. Rousseau, M. J. O'Hagan, W. G. Dougherty, W. S. Kassel, D. L. DuBois and R. M. Bullock, *Chem. Commun.*, 2011, **47**, 12212-12214.
38. D. E. Prokopchuk, E. S. Wiedner, E. D. Walter, C. V. Popescu, N. A. Piro, W. S. Kassel, R. M. Bullock and M. T. Mock, *J. Am. Chem. Soc.*, 2017, **139**, 9291-9301.
39. T. Liu, Q. Liao, M. O'Hagan, E. B. Hulley, D. L. DuBois and R. M. Bullock, *Organometallics*, 2015, **34**, 2747-2764.
40. T. Liu, D. L. DuBois and R. M. Bullock, *Nat. Chem.*, 2013, **5**, 228-233.
41. M. Fang, E. S. Wiedner, W. G. Dougherty, W. S. Kassel, T. Liu, D. L. DuBois and R. M. Bullock, *Organometallics*, 2014, **33**, 5820-5833.
42. A. Bondi, *J. Phys. Chem.*, 1964, **68**, 441-451.
43. R. S. Rowland and R. Taylor, *J. Phys. Chem.*, 1996, **100**, 7384-7391.
44. G. M. Jacobsen, R. K. Shoemaker, M. J. McNevin, M. Rakowski DuBois and D. L. DuBois, *Organometallics*, 2007, **26**, 5003-5009.

45. M. Bautista, K. A. Earl, R. H. Morris and A. Sella, *J. Am. Chem. Soc.*, 1987, **109**, 3780-3782.
46. A. E. Reed, L. A. Curtiss and F. Weinhold, *Chem. Rev.*, 1988, **88**, 899-926.
47. K. D. Welch, W. G. Dougherty, W. S. Kassel, D. L. DuBois and R. M. Bullock, *Organometallics*, 2010, **29**, 4532-4540.
48. L. Brammer, *Dalton Trans.*, 2003, 3145-3157.
49. N. V. Belkova, L. M. Epstein, O. A. Filippov and E. S. Shubina, *Chem. Rev.*, 2016, **116**, 8545-8587.
50. L. M. Epstein, E. S. Shubina, A. N. Krylov, A. Z. Kreindlin and M. I. Rybinskaya, *J. Organomet. Chem.*, 1993, **447**, 277-280.
51. E. Peris and R. H. Crabtree, *Chem. Commun.*, 1995, 2179-2180.
52. V. A. Levina, O. A. Filippov, E. I. Gutsul, N. V. Belkova, L. M. Epstein, A. Lledos and E. S. Shubina, *J. Am. Chem. Soc.*, 2010, **132**, 11234-11246.
53. N. V. Belkova, E. I. Gutsul, O. A. Filippov, V. A. Levina, D. A. Valyaev, L. M. Epstein, A. Lledos and E. S. Shubina, *J. Am. Chem. Soc.*, 2006, **128**, 3486-3487.
54. A. D. Wilson, R. K. Shoemaker, A. Miedaner, J. T. Muckerman, D. L. DuBois and M. Rakowski DuBois, *Proc. Natl. Acad. Sci. U.S.A.*, 2007, **104**, 6951-6956.
55. J. Y. Yang, S. E. Smith, T. Liu, W. G. Dougherty, W. A. Hoffert, W. S. Kassel, M. R. DuBois, D. L. DuBois and R. M. Bullock, *J. Am. Chem. Soc.*, 2013, **135**, 9700-9712.
56. E. S. Wiedner, J. Y. Yang, S. T. Chen, S. Raugei, W. G. Dougherty, W. S. Kassel, M. L. Helm, R. M. Bullock, M. Rakowski DuBois and D. L. DuBois, *Organometallics*, 2012, **31**, 144-156.
57. J. Y. Yang, R. M. Bullock, W. J. Shaw, B. Twamley, K. Fraze, M. Rakowski DuBois and D. L. DuBois, *J. Am. Chem. Soc.*, 2009, **131**, 5935-5945.
58. A. Kochem, M. O'Hagan, E. S. Wiedner and M. van Gastel, *Chem. - Eur. J.*, 2015, **21**, 10338-10347.
59. G. R. Fulmer, A. J. M. Miller, N. H. Sherden, H. E. Gottlieb, A. Nudelman, B. M. Stoltz, J. E. Bercaw and K. I. Goldberg, *Organometallics*, 2010, **29**, 2176-2179.
60. B. J. Hathaway, D. G. Holah and A. E. Underhill, *J. Chem. Soc.*, 1962, 2444-2448.
61. R. A. Heintz, J. A. Smith, P. S. Szalay, A. Weisgerber and K. R. Dunbar, *Inorg. Synth.*, 2002, **33**, 75-83.

62. K. Fraze, A. D. Wilson, A. M. Appel, M. Rakowski DuBois and D. L. DuBois, *Organometallics*, 2007, **26**, 3918-3924.
63. APEX II (v. 2009.3), Bruker AXS, 2009.
64. Sheldrick, G. M. SHELXTL, Version 6.14; Bruker AXS Inc., Madison, WI, 2004.
65. A. D. Becke, *Phys. Rev. A*, 1988, **38**, 3098-3100.
66. J. P. Perdew, *Phys. Rev. B*, 1986, **33**, 8822-8824.
67. C. S. Letko, J. A. Panetier, M. Head-Gordon and T. D. Tilley, *J. Am. Chem. Soc.*, 2014, **136**, 9364-9376.
68. S. Grimme, S. Ehrlich and L. Goerigk, *J. Comp. Chem.*, 2011, **32**, 1456-1465.
69. S. Grimme, *J. Comp. Chem.*, 2006, **27**, 1787-1799.
70. M. M. Francl, W. J. Pietro, W. J. Hehre, J. S. Binkley, M. S. Gordon, D. J. Defrees and J. A. Pople, *J. Chem. Phys.*, 1982, **77**, 3654-3665.
71. W. J. Hehre, R. Ditchfield and J. A. Pople, *J. Chem. Phys.*, 1972, **56**, 2257-2261.
72. J. M. L. Martin and A. Sundermann, *J. Chem. Phys.*, 2001, **114**, 3408-3420.
73. A. V. Marenich, C. J. Cramer and D. G. Truhlar, *J. Phys. Chem. B*, 2009, **113**, 6378-6396.
74. F. Neese, *Wiley Interdiscip. Rev. Comput. Mol. Sci.*, 2018, **8**, e1327.
75. K. S. Thanthiriwatte, E. G. Hohenstein, L. A. Burns and C. D. Sherrill, *J. Chem. Theory Comput.*, 2011, **7**, 88-96.
76. G. M. Chambers, S. I. Johnson, S. Raugei and R. M. Bullock, *Chem. Sci.*, 2019, **10**, 1410-1418.
77. E. D. Glendening, J. K. Badenhoop, A. E. Reed, J. E. Carpenter, J. A. Bohmann, C. M. Morales, C. R. Landis and F. Weinhold, *NBO 6.0.*, Theoretical Chemistry Institute, Univeristy of Wisconsin, Madison, 2013.